Population transfer at periodically repeated level crossings

B. M. Garraway and S. Stenholm
Research Institute for Theoretical Physics, Siltavuorenpenger 20C, SF-00170 Helsinki, Finland
(Received 6 May 1991)

We have explored a genuinely time-dependent problem consisting of periodic crossings of energy levels. The model can be realized in several physical systems, but we refer it explicitly to a two-level ion that swings in a harmonic trap and concurrently interacts with a traveling light wave. We have solved the Schrödinger equation for this model by numerical integration as well as by the use of matrix continued fractions for the steady state. We investigate both the time and the frequency behavior of the model. We have also compared the exact behavior with an intuitive model based on a Landau-Zener description of each crossing followed by a simple relaxation behavior. In addition, the coherent interaction with the field is found to lead to a resonancelike behavior of the population transfer, which we can attribute to the accumulated phase of the Bloch vector. The various time scales of the problem are identified and their physical significance is elucidated.

PACS number(s): 32.80.Bx, 33.80.Ps

I. INTRODUCTION

In quantum physics, there are very few systems that can be followed in time while they undergo their quantal evolution. Recent techniques, however, allow one to isolate individual atoms in traps and track their behavior in real time. This may afford an opportunity to test the time evolution of quantum-mechanical systems in a regime not earlier available to experimentalists.

In this paper we discuss the simple model of an atomic two-level system periodically tuned into and out of resonance with a monochromatic field supplied by a laser. One possible realization is a harmonically trapped atom (or ion), see Fig. 1(a), which is Doppler shifted through its resonance by the periodic motion. In Fig. 1(b) we show the oscillating atomic energy difference regularly coinciding with the laser frequency. At the periodically occurring level crossings, we find a mixing of the states, which in the adiabatic limit effects a complete transfer of population between the levels. The nonadiabatic corrections can be estimated from the treatment of Landau [1] and Zener [2] as was suggested in Ref. [3]. If the lifetime of the upper level is short compared with the oscillational period in the trap, the excited state will decay before the next crossing appears, and observing the outgoing photons, we will see a series of regularly spaced bursts of energy as indicated in Fig. 1(c). In Ref. [4] it was suggested that this could be used as a single-atom clock. The suggestion was motivated by the fact that periodic phenomena are commonplace in quantum systems but the reading of a microscopic clock may in itself pose a physical problem.

It is easy to envisage other physical systems where periodic modulation of the energy levels occurs. When atoms travel in periodic structures, e.g., in channeling, their levels will be affected by the background lattice. Also artificial optical structures, fibers [5,6], and superlattices may offer periodic modulations leading to repeated level crossings. In laser-cooling experiments, the standing wave structures give rise to periodic light shifts that play an essential role [7–9]. In some atomic investigations [10] the external fields are modulated periodically to facilitate the experiments.

We have found it interesting to investigate the details of the physical situation described above. We try to see what the observable phenomena are like, to what extent their behavior can be understood in terms of simple models, and which parameter ranges introduce noticeable modifications to the simplest behaviors. In addition, the system offers some opportunities to test computational models that are based on intuitive concepts against detailed calculations. Some of the features found may be verifiable or even significant in atomic physics. In particular we find a novel physical system where the Landau-Zener behavior can be subjected to an experimental test.

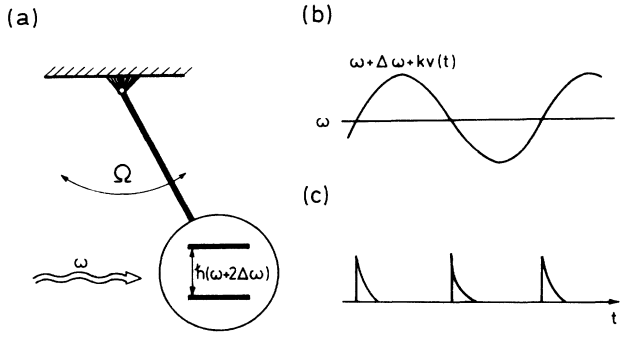

FIG. 1. The physical situation considered in this paper is presented. (a) A harmonically oscillating two-level system under the influence of a laser field nearly resonant with the level spacing. The Doppler shift modulates this spacing so that it coincides with the laser frequency periodically (b). At each crossing the two-level system becomes excited, and for a short enough lifetime the excitation energy is seen to leave the atom spontaneously (c).

II. THE THEORETICAL TREATMENT

A. Setting up the model

We assume a traveling laser wave of frequency ω and wave vector k to impinge on a simple two-level atom with the energy-level difference $\hbar(\omega+2\Delta\omega)$. In the rotating-wave approximation the detuning for a periodically Doppler shifted atomic particle is

$$\Delta E/\hbar=2\Delta\omega+kv(t)$$
$$=2\Delta\omega+kv_0\cos\Omega t\ . \tag{2.1}$$

Using the Pauli matrices σ_i $(i=1,2,3)$ we can write the Hamiltonian in the form

$$H/\hbar=(\Delta\omega+A\cos\Omega t)\sigma_3+V\sigma_1\ , \tag{2.2}$$

where $\hbar V$ is the (dipole) coupling between the energy levels and A is the oscillational amplitude as determined from Eq. (2.1). We define the optical Bloch vector $\vec{r}$, using the 2×2 density matrix ρ as

$$\begin{aligned} r_1&=\rho_{12}+\rho_{21}\ ,\\ r_2&=i(\rho_{12}-\rho_{21})\ ,\\ r_3&=\rho_{22}-\rho_{11}\ . \end{aligned} \tag{2.3}$$

With the Hamiltonian (2.2) we find the equations of motion

$$\begin{aligned} \frac{d}{dt}r_1&=-2(\Delta\omega+A\cos\Omega t)r_2-\gamma r_1\ ,\\ \frac{d}{dt}r_2&=2(\Delta\omega+A\cos\Omega t)r_1-2Vr_3-\gamma r_2\ ,\\ \frac{d}{dt}r_3&=2Vr_2-\gamma_0 r_3-\lambda_p\ . \end{aligned} \tag{2.4}$$

Here γ and γ_0 are the transverse and longitudinal relaxation rates, respectively, and λ_p is an externally imposed pumping rate. This may be taken to be $\mp\gamma_0$ if the atoms are introduced in the upper or lower state, respectively. We note that changing λ_p achieves only a simple scaling of the Bloch vector components. Here we have assumed that both levels are emptied to lower unobserved levels; if level 1 is the ground state or a metastable state, the dominating decay mechanism may be spontaneous emission between the levels. In that case $\gamma_0\leq2\gamma$. As long as the decay rates are of the same order, our physical conclusions will not be affected. Hence we have used $\gamma_0=\gamma$ in our numerical calculations.

Starting with given initial conditions, we can integrate the set of equations (2.4) to obtain its time evolution. For this purpose we have employed either the fifth-order Runge-Kutta [11] or one of its variations. The results are used in the following sections to check the validity of our other treatments and to estimate the accuracy of the approximations.

B. The steady-state description

In the steady state, the time evolution of the Bloch vector must display the periodicity of the external field, and hence we introduce an ansatz where each of its components r_j $(j=1,2,3)$ is expanded in a Fourier series

$$r_j=\sum_{n=-\infty}^{+\infty}R_j(n)\exp(in\Omega t)\ . \tag{2.5}$$

Substituting this ansatz into the Bloch equations (2.4) we find a set of three coupled recurrence relations for the Fourier amplitudes of the harmonics $R_j(n)$, namely

$$(in\Omega+\gamma)R_1(n)=-2\Delta\omega R_2(n)$$
$$-A[R_2(n+1)+R_2(n-1)]\ , \tag{2.6}$$

$$(in\Omega+\gamma)R_2(n)=2\Delta\omega R_1(n)$$
$$+A[R_1(n+1)+R_1(n-1)]$$
$$-2VR_3(n)\ , \tag{2.7}$$

$$(in\Omega+\gamma_0)R_2(n)=2VR_2(n)-\lambda_p\delta_{n0}\ . \tag{2.8}$$

Using a fairly standard procedure [12] these can be rewritten in terms of matrices and solved in terms of matrix continued fractions. The procedure can be simplified by solving for R_3 from (2.8) and introducing this into Eq. (2.7). Defining the vector

$$\mathbf{R}_n=\begin{bmatrix}R_1(n)\\R_2(n)\end{bmatrix}\ , \tag{2.9}$$

we can write Eqs. (2.6)–(2.8) in the matrix form

$$\mathbf{R}_n=\mathbf{B}\delta_{n0}+\underline{C}_n(\mathbf{R}_{n+1}+\mathbf{R}_{n-1})\ , \tag{2.10}$$

where $\mathbf{B}$ is a vector and $\underline{C}_n$ is a 2×2 matrix. Their expressions are given in the Appendix, where we also give the details of the solution used in this section. To solve (2.10) we define the transfer matrices $\underline{T}_n$ by setting

$$\mathbf{R}_n=\underline{T}_n\mathbf{B}\ . \tag{2.11}$$

For these we can obtain matrix continued fractions that can be evaluated in a straightforward way numerically; see the Appendix for details.

We note that at resonance $\Delta\omega=0$, Eqs. (2.6)–(2.8) imply that R_2 and R_3 have only even components and R_1 only odd ones. It is then possible to evaluate the Bloch vector in terms of an ordinary continued fraction instead of a matrix one, which speeds up the computational procedure considerably.

In Fig. 2 we show a result of the evaluation of the time-dependent Bloch vector. We start the integration from the externally imposed initial value $r_3=1$, i.e., an inverted population. The solid line shows the transient approach to the periodic steady-state behavior. The oscillating dotted line shows the Fourier transform solution obtained from the continued fractions. In this case only four harmonics have been included, but we see that after a transient period of the order of a few relaxation time constants γ^{-1}, the solutions agree well. The time-averaged inversion is given by $R_3(0)$, which is shown as a

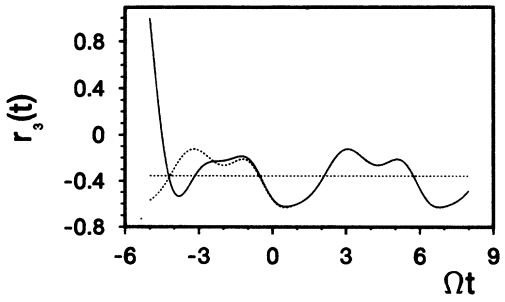

FIG. 2. The time evolution of the population difference $r_3(t)$ when the two oscillating levels are detuned from the laser. The result from the numerical integration is shown by the solid curve, that from the continued fraction as the dashed curve (in this case using four harmonics only). The horizontal dashed line is the time-averaged population obtained from the continued fractions. The system starts from $\Omega t=-5$, and it rapidly approaches the steady-state behavior described by the continued-fraction result. The highly nonsymmetric steady-state behavior is caused by the detuning $\Delta\omega=0.5\Omega$, which is 50% of the driving amplitude $A=\Omega$. The coupling is $V=\Omega$, and the decay rate is $\gamma=\Omega$. The two remaining parameters needed are $\gamma=\gamma_0$ and $\lambda_p=\Omega$; these will remain the same in all following figures. Only this figure shows the relaxation towards the steady state.

horizontal line in Fig. 2.

For other values of the parameters, the time evolution contains many more features. Figure 3 shows a case where the sudden excitation at the crossing is followed by an exponential decay overlapped by a rapid oscillation due to the precession of the Bloch vector; cf. the expected behavior in Fig. 1(c). In Fig. 3 the solid line is the result of exact numerical integration and the dotted line is the Fourier synthesis based on 30 harmonics. Including more than 34 harmonics leads to such a small difference

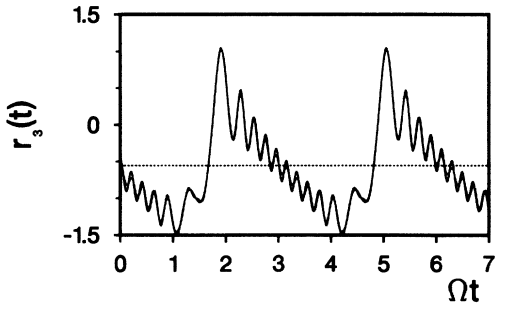

FIG. 3. The steady-state evolution of $r_3(t)$ (solid curve) for parameters chosen to show a higher level of excitation and more oscillations. The continued fraction solution, with 30 harmonics, is shown as the dotted curve. If more than 34 harmonics are included, the two solutions coincide. The horizontal line is the continued-fraction time average. The parameters are $A=16\Omega$ and $V=3\Omega$. The relaxation has been reduced to $\gamma=0.3\Omega$. There is no detuning; $\Delta\omega=0$.

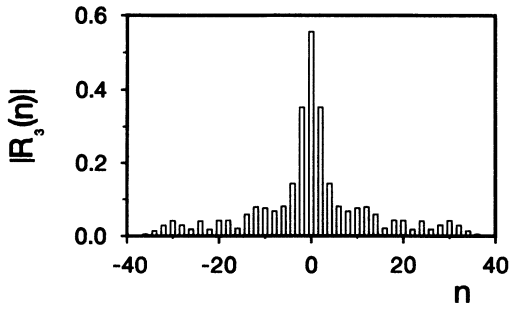

FIG. 4. The spectrum of the steady-state time evolution of Fig. 3. The absolute value of each harmonic is plotted. Note that the value for $n=0$ is the time average, which is actually negative. The spectrum is mainly confined to the range $|n|\leq 40$.

that it cannot be seen in the figure. The dotted horizontal line is the average inversion. We will discuss the precessional oscillations in Sec. III C.

To see the influence of the higher harmonics, we plot the absolute value of the components $R_3(n)$ in Fig. 4. It can be seen that the spectrum is contained within ± 40 harmonics. In this case, the odd harmonics are missing, because we look at $\Delta\omega=0$.

It turns out that the basic features of Figs. 2 and 3 can be understood from simple physical considerations. These will be introduced in the next section.

III. RESULTS AND INTERPRETATION

A. Simple adiabatic description

The Bloch equations (2.4) can be written in vector form (with $\gamma_0=\gamma$ for simplicity)

$$\frac{d}{dt}\vec{r}=\vec{m}\times\vec{r}-\gamma\vec{r}-\lambda_p\hat{e}_3\ , \tag{3.1}$$

where $\vec{r}$ is the three-vector with the components (2.3) and $\vec{m}$ is the pseudofield vector

$$\vec{m}=2V\hat{e}_1+2(\Delta\omega+A\cos\Omega t)\hat{e}_3\ . \tag{3.2}$$

The unit vectors $\hat{e}_i$ $(i=1,2,3)$ span the spin space where the Bloch vector resides.

Neglecting pumping and relaxation in Eq. (3.1), we find that the Bloch vector precesses around the direction of the pseudofield $\vec{m}$ with the angular frequency $|\vec{m}|$. This holds true even when the field changes direction slowly, which is called adiabatic following in magnetic resonance. When we approach a crossing, the field vector moves rapidly because of the vanishing value of its third-component. As a result a difference arises between the directions of the Bloch vector and the field vector. After the crossing it determines the precession that can be seen as an oscillation of the third-component of the Bloch vector. Redistribution of the population on the two levels occurs during the crossing. From the excited state, the Bloch vector relaxes by a spiraling motion as both the precessional motion and the level of excitation damp out. In time, an equilibrium position is reached before the

next crossing excites the system again.

The exchange of population between two crossing levels is just the situation described by Landau [1] and Zener [2]. In order to apply their methods, we assume that the crossing time is so short that we may neglect pumping and decay while the crossing takes effect. The Hamiltonian (2.2) can be linearized for an interval small enough near the crossing, giving the standard form

$$H=\hbar\begin{bmatrix}-\lambda\Delta t & V\\ V & \lambda\Delta t\end{bmatrix} . \tag{3.3}$$

The time variable Δt is the deviation from the crossing times determined by

$$\Delta\omega + A\cos\Omega t = 0 . \tag{3.4}$$

At these crossings we can determine the parameter λ from

$$\lambda=\pm\Omega\sqrt{A^2-\Delta\omega^2} ; \tag{3.5}$$

the sign depends on the direction of traversing the crossing.

The Hamiltonian (3.3) can be treated by the Landau-Zener calculation, which shows that the mixing of the levels takes place over a time scale determined by

$$t_c=\frac{V}{\lambda} . \tag{3.6}$$

The solution of the problem is given in terms of the adiabaticity parameter

$$\Lambda=\frac{V^2}{\lambda} . \tag{3.7}$$

Starting from the inversion $r_3(-\infty)=-1$, one obtains from the Landau-Zener treatment the final result

$$r_3(+\infty)=1-2\exp(-\pi\Lambda) . \tag{3.8}$$

When the process takes place infinitesimally slowly, $\lambda\Longrightarrow 0$, the population is totally inverted during the adiabatic passage.

Armed with these tools we can make a simple analytic model of the periodic sequence of the time evolution. We neglect the coherent precession about the pseudofield vector (see Sec. III C) and describe the evolution simply in terms of the third component of the Bloch vector (the population inversion).

For simplicity we consider the case $\Delta\omega=0$, and denote the time between the level crossings as

$$T_{1/2}=\frac{\pi}{\Omega} . \tag{3.9}$$

Our intuitive picture is based on the situation where we assume

$$T_{1/2}>\gamma_0^{-1}>t_c . \tag{3.10}$$

These conditions are discussed in Secs. III B and IV.

Just before a crossing, at the time $\Delta t=-\delta t$ the inversion is $r_3(-\delta t)$ (for any $\delta t>t_c$), which according to the result (3.8) becomes

$$r_3(\delta t)=-r_3(-\delta t)(1-2e^{-\pi\Lambda}) , \tag{3.11}$$

after the crossing. Having passed this, the Bloch vector will precess under the influence of pumping and damping. In our model we only treat the average inversion by retaining from the full Bloch equations (with $\gamma_0=\gamma$)

$$\frac{d}{d\Delta t}r_3=-\gamma r_3+\lambda_p . \tag{3.12}$$

With (3.11) as the initial condition we find the solution

$$r_3(\Delta t)=-\frac{\lambda_p}{\gamma}(1-e^{-\gamma(\Delta t-\delta t)})+r_3(\delta t)e^{-\gamma(\Delta t-\delta t)} . \tag{3.13}$$

After the time $(T_{1/2}-2\delta t)$ the next crossing is encountered, and in the steady state, we require

$$r_3(T_{1/2}-\delta t)=r_3(-\delta t) . \tag{3.14}$$

Using Eqs. (3.11) and (3.13) and letting $\delta t\Longrightarrow 0$ we find the result

$$r_3(+0)=\frac{\lambda_p}{\gamma}\left[-1+\frac{\exp(\gamma T_{1/2})}{1+\dfrac{\exp(\gamma T_{1/2})-1}{2[1-\exp(-\pi\Lambda)]}}\right] . \tag{3.15}$$

We can substitute the result (3.15) into Eq. (3.13) and find the population at times $0<\Delta t<T_{1/2}$

$$r_3(\Delta t)=\frac{\lambda_p}{\gamma}\left[-1+\frac{\exp(\gamma T_{1/2}-\gamma\Delta t)}{1+\dfrac{\exp(\gamma T_{1/2})-1}{2[1-\exp(-\pi\Lambda)]}}\right] . \tag{3.16}$$

Using (3.15) and (3.16) we can derive an expression for the population transfer at the crossing

$$\Delta r_3=r_3(+0)-r_3(T_{1/2})=\frac{\lambda_p}{\gamma}\left[\frac{1}{\dfrac{1}{\exp(\gamma T_{1/2})-1}+\dfrac{1}{2[1-\exp(-\pi\Lambda)]}}\right] . \tag{3.17}$$

This simple equation shows how the population transfer depends on the two parameters $\gamma T_{1/2}$ and $\pi\Lambda$ that characterize the decay and the adiabatic transfer, respectively. It can be used in the limit of fast decay $\gamma\Longrightarrow\infty$ in accordance with the conditions (3.10).

From Eq. (3.16) we can derive the average inversion over the time $T_{1/2}$ to be

$$\bar{r}_3=\frac{\lambda_p}{\gamma}\left[-1+\frac{\exp(\gamma T_{1/2})-1}{\gamma T_{1/2}}\times\left[1+\frac{\exp(\gamma T_{1/2})-1}{2[1-\exp(-\pi\Lambda)]}\right]^{-1}\right] . \tag{3.18}$$

In the limit of strong damping (i.e., for $\gamma T_{1/2}\gg 1$) we find

$$\bar{r}_3\Longrightarrow-\frac{\lambda_p}{\gamma}\left[1-\frac{2}{\gamma T_{1/2}}[1-\exp(-\pi\Lambda)]\right] . \tag{3.19}$$

B. Comparison with numerical results

The time dependence (3.16) combined with the Landau-Zener jump (3.17) at the crossings makes it possible to plot the time evolution of the population inversion as described by the simple model of the previous section. In this section we are going to compare this evolution with the one obtained from the exact numerical results described in Sec. II.

In Figs. 5–7 we fix the adiabaticity parameter at the crossing to the value $\Lambda=0.22$, which gives about 50% population transfer according to the Landau-Zener theory. The decay rates are taken to be equal, $\gamma=\gamma_0$, and the detuning is zero, $\Delta\omega=0$.

In Fig. 5 the parameter characterizing the decay is $\gamma T_{1/2}=\pi\gamma/\Omega=\pi/2$, and the parameter characterizing the crossing is $\Omega t_c=\frac{1}{20}$. In this situation the level-crossing excitation is rather sudden but the decay is not complete between the crossings. The figure shows the approximate theory (dashed line) and the exact numerical result (solid line). The most striking difference is the oscillations deriving from the precession of the Bloch vector around the field vector; this feature is missing from our approximate theory. The figure also shows the average level of excitation (3.18) (the dashed horizontal line) and the corresponding exact value $R_3(0)$ (the dotted horizontal line) from the continued fraction evaluation (see the Appendix); the discrepancy found between these two values is discussed in Sec. III C. We can see that the time-evolution curve is well represented by the approximate result when this is shifted to make the averages agree (the dotted curve). In particular the jump at the level crossing seems to be well provided by the Landau-Zener theory.

In Fig. 6 the parameters are as in Fig. 5, but the decay rate γ is increased by one order of magnitude. Then the precessional oscillations are rapidly damped out, and the decay process has time to run its course between the crossings. However, the decay time now approaches the level-crossing time scale $\gamma t_c=\frac{1}{4}$, and the excitation is no longer sudden but smeared out. The approximate theory does, however, describe the time evolution rather well; in particular the averaged level populations coincide in this case.

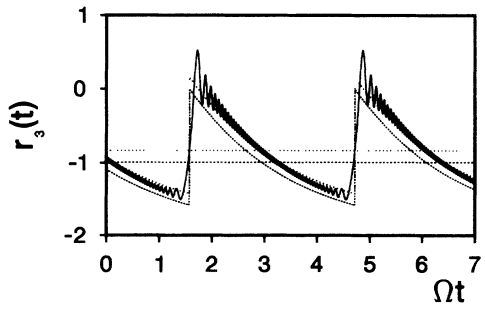

FIG. 5. The solid curve shows the integrated result for the population inversion for the parameters $\Lambda=0.22$, $\Omega t_c=0.05$, and $\gamma=0.5\Omega$ ($\Delta\omega=0$). Λ and t_c are defined in Eqs. (3.7) and (3.6), respectively. The dashed sawtooth-shaped curve is the prediction from Eq. (3.13). The horizontal dashed line is its average (3.18). The higher dotted line is the actual value of the mean inversion from the continued-fraction method. The upper, dotted sawtooth represents the result of shifting the prediction (3.13) so that its average coincides with the correct one; thus shifted, the simple theory shows quite a good fit to the numerical results when the rapid oscillations are smeared out.

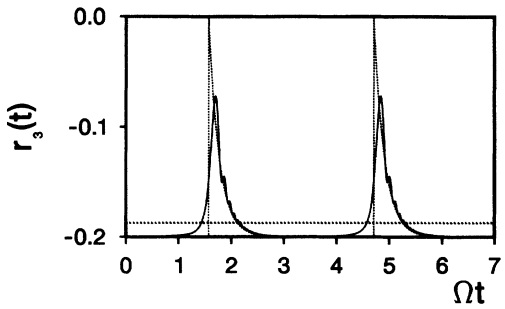

FIG. 6. The same as Fig. 5, but with the damping increased to $\gamma=5\Omega$. The average inversion from the continued fractions and from the simple theory now almost agree. Thus the simple sawtooth needs no shifting to give good agreement.

In Fig. 7 we have increased the decay rate by another factor of 10; the level-crossing time scale and the decay rate are similar, $\gamma t_c=2.5$, and the simple theory loses sense.

The intuitive picture given in Fig. 1(c) can be realized in the adiabatic limit when Ωt_c is small. Choosing the parameters such that $\Lambda=1.0$, we find the result in Fig. 8. Because here $\gamma T_{1/2}=\pi\gamma/\Omega=5\pi$, the decay is well completed between the level crossings, and in addition, $\gamma t_c=\frac{1}{4}$, which implies that the decay of the levels does not interfere with the crossing points. In this case the approximate solution can hardly be distinguished from the numerical results.

An instructive way to test the accuracy of the approximation developed in Sec. III A is to look at the Fourier

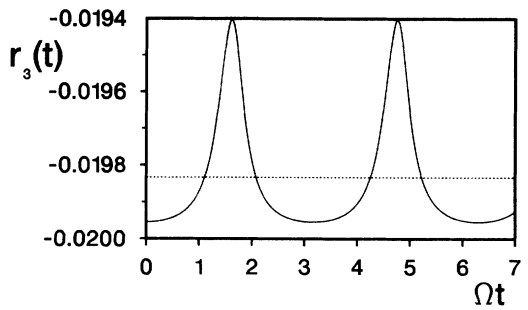

FIG. 7. Similar to Figs. 5 and 6 but with the damping increased to $\gamma=50\Omega$. The strong dissipation leads to a low-average level of excitation. The time dependence needs only a few harmonics, and it makes no sense to apply the theory of Sec. III A. Only the numerical result (solid curve) and the computed mean (dashed line) are shown.

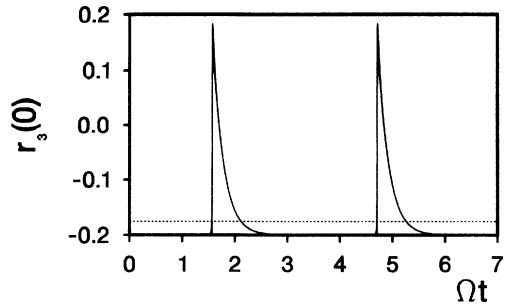

FIG. 8. An example of where the theory of Sec. III A is truly applicable. The parameters are $\Lambda=1$, $\Omega t_c=0.005$, and $\gamma=5\Omega$ ($\Delta\omega=0$). The numerical curve (solid) agrees with the theory (dotted curve) almost perfectly. The horizontal dashed line is the average inversion.

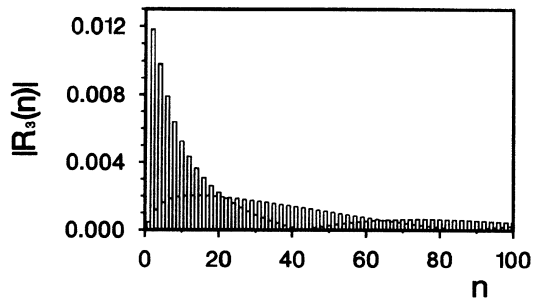

FIG. 10. The spectrum for a case with detuning $\Delta\omega=80\Omega$. Both odd and even harmonics are present in $R_3(t)$. Both sequences are seen to be modulated. The parameters are $\Lambda=0.22$, $\Omega t_c=0.01$, and $\gamma=5\Omega$. The detuning is only 3.6% of the driving amplitude A. The $n=0$ component is omitted for clarity [$R_3(n=0)=-0.1872$].

spectrum of the solutions. The continued-fraction method generates this directly, and the Fourier coefficients are obtained from our simple theory by inverting the expansion

$$r_3(t)=\sum_{n\ \text{even}} R_3^{\mathrm{LZ}}(n)\exp(i\pi nt/T_{1/2})\ . \tag{3.20}$$

Inserting $r_3(t)$ as given between two crossings by (3.16), we find the coefficients

$$R_3^{\mathrm{LZ}}(n)=\frac{(-1)^{n/2}\Delta r_3}{\gamma T_{1/2}+i\pi n}-\delta_{n0}\frac{\lambda_p}{\gamma}\ . \tag{3.21}$$

In Fig. 9 we plot the absolute value of the coefficients (3.21) (dotted bars) and the exact ones obtained from the continued-fraction treatment (solid bars). As we can see there is general agreement between the two sets of coefficients. The small value of $\gamma T_{1/2}$ used here allows the various crossings to interfere with each other during the time evolution, and this manifests itself in ripples in the spectrum. If $\gamma T_{1/2}$ or Λ is increased, the ripples disappear and the agreement improves.

Because $\Delta\omega=0$ in Fig. 9, only the even coefficients are present. Our continued-fraction method can solve for the time evolution even when the resonance is detuned. We have explored this case numerically and looked at the consequences of detuning. The spectrum acquires odd harmonics, because of the asymmetry between the crossings. An example is shown in Fig. 10, where, in addition to the even harmonics behaving similarly to those in Fig. 9, a series of odd harmonics arises. Both series show modulations that make each one fall to near zero and then rise again. For the parameters chosen, however, the detuning only causes a slight shift in the time positions of the individual pulses. Bringing the detuning $\Delta\omega$ up near A, makes the two separate peaks of each full period merge into one single rounded peak of reduced amplitude.

From Eq. (3.21) we can see that each Fourier coefficient with $|n|>0$ is proportional to the population transfer at the level crossing. This is a feature of the theory that tests the validity of the Landau-Zener treatment, and therefore it is of interest to try to extract this information from the numerical results. In Fig. 11 we

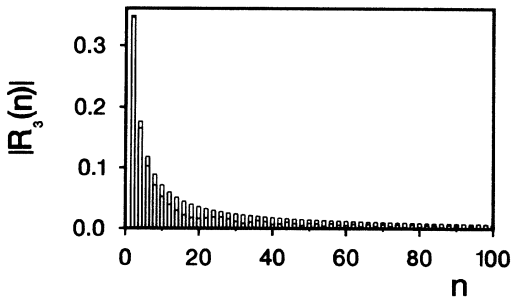

FIG. 9. This shows a Fourier spectrum with ripples in the amplitudes. We plot the absolute values with the steady-state component $n=0$ omitted for clarity [$R_3(0)=-0.4999$]. The parameters are $\Lambda=0.5$, $\Omega t_c=0.1$, and $\gamma=0.5\Omega$ ($\Delta\omega=0$). The modulation in the spectrum derives from the interference between the crossings. The dotted bars show the spectrum predicted in Sec. III A; that theory cannot reproduce the modulation.

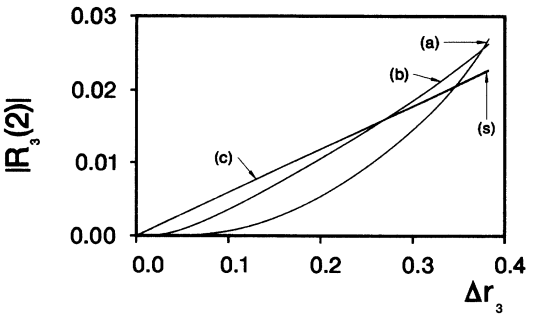

FIG. 11. A plot of the amplitude of the second harmonic as a function of the theoretically obtained jump at the crossing Δr_3 as given by Eq. (3.17). The change in Δr_3 is effected by varying only Λ. The other parameters are $\gamma=5\Omega$, $\Delta\omega=0$, and (*a*) $\Omega t_c=0.2$, (*b*) $\Omega t_c=0.1$, (*c*) $\Omega t_c=0.01$. The dotted curve marked (*s*) arises from the simple theory of Sec. III A; it consists of the linear relation (3.21) for $n=2$.

plot the second harmonic ($n=2$) as a function of the population transfer expected from the Landau-Zener treatment with the crossing time scale t_c as the parameter. The simple result (3.21) gives the straight line marked (s). We see that for $\gamma t_c=1.0$ (a) and $\gamma t_c=0.5$ (b) there is no agreement; for $\gamma t_c=0.05$ (c) we find good agreement. A small value of γt_c indicates that the crossing is fast compared with the relaxation, and then we expect the Landau-Zener treatment to hold.

C. Coherence effects between crossings

In our previous theoretical treatment we have assumed that the relaxation rates are large enough to restore the Bloch vector to near equilibrium in the time between the crossings. Then no coherence effects between the crossings need be included in the treatment. We are now going to consider the case when the system relaxes more slowly than the recurrence of the crossings, i.e.,

$$\gamma T_{1/2} \leq 1 \ . \tag{3.22}$$

In this case the Bloch vector remembers the previous level crossing when it encounters a new one, which means that the density matrix retains some off-diagonal elements between the crossings. The precessional motion of the Bloch vector resides in these coherences, and they cause the wiggles in the numerically obtained curves in Figs. 3 and 5. When the condition (3.22) holds, the oscillations persist to the next crossing and affect the level transfer.

To understand the role of the coherences, we have to add the precessional motion to the simple model in Sec. III A. The initial value for the Bloch vector entering a crossing is not only determined by the pumping and decay, but it will also depend on the oscillational phase of the vector entering the crossing region. When the decay is slow enough, this will be a major factor in determining the actual transfer that takes place. As a function of the parameters of the problem, we thus expect to see widely varying behavior. This is, indeed, seen in Fig. 12 where we plot the mean population $R_3(0)$ as a function of the crossing time scale $t_c=V/\lambda$. For fast crossings we see a series of sharp dips in the average transfer, which indicate the role of the oscillating phase. Incidentally, we note that these large dips are responsible for the shift of the average levels between the simple model and the numerical results that are seen in Fig. 5.

To substantiate our explanation of the dips seen in Fig. 12, we assume full adiabatic following during the time between crossings. The Bloch vector then precesses around the instantaneous pseudofield vector, which has the magnitude [see Eq. (3.2)]

$$|\vec{m}|=2\sqrt{V^2+A^2\cos^2\Omega t}$$
$$=2\frac{\Lambda}{t_c}\sqrt{1+\cos^2\Omega t/\Omega^2 t_c^2} \ . \tag{3.23}$$

Using this result, we can calculate the phase accumulated between the crossings from the integral

$$\Phi(\Lambda,t_c)=\int_{-T_{1/2}/2}^{T_{1/2}/2}|\vec{m}(t)|dt$$
$$=4\Lambda\frac{\sqrt{1+(\Omega t_c)^2}}{(\Omega t_c)^2}\mathcal{E}(\kappa) \ , \tag{3.24}$$

where the argument

$$\kappa=\frac{1}{\sqrt{1+(\Omega t_c)^2}} \tag{3.25}$$

occurs in the Legendre elliptic function of the second kind

$$\mathcal{E}(\kappa)=\int_0^{\pi/2}\sqrt{1-\kappa^2\sin^2 x}\,dx \ . \tag{3.26}$$

It seems reasonable to assert that in all those cases where we arrive at a crossing with the same accumulated phase, the resulting population transfer would be the same. Thus if we choose to concentrate on combinations of Λ and t_c such that

$$\Phi(\Lambda,t_c)=2\pi n \quad (n=1,2,3,4,\ldots) \ , \tag{3.27}$$

we expect these to lead to the same average transfer of population and hence the same average $R_3(0)$. In Fig. 13 we display this average as a surface over the $\Lambda,\Omega t_c$ plane. The ridges and valleys occur because certain phase angles would make periodic evolution impossible unless the system adjusts self-consistently. The lines in Fig. 13 show the solutions of Eq. (3.27) projected onto the surface. We see that they nearly coincide with the bottoms of the valleys in the calculated function. If we cut the surface at a constant Λ, we find an oscillating behavior like that shown in Fig. 12. (To make the lines visible in Fig. 13 we have chosen the parameter γ such that variations in the surface are not too large.) The positions of the resonances estimated from Eqs. (3.24) and (3.27) are indicated

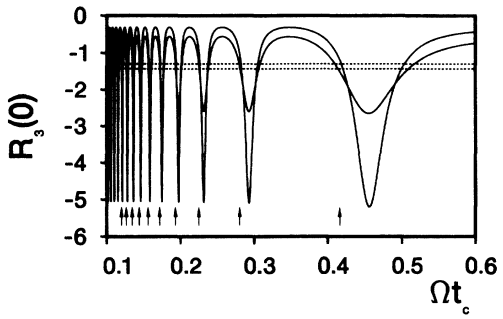

FIG. 12. The average inversion (from the continued-fraction method) as a function of the crossing width Ωt_c. The curve with sharper dips has $\gamma=0.1\Omega$, and the other curve has $\gamma=0.2\Omega$. Other parameters are $\Lambda=0.22$ and $\Delta\omega=0$. The dashed lines give the result calculated in Sec. III A; they are not dependent on Ωt_c in that theory. The lower dashed line is for $\gamma=0.1\Omega$. The arrows mark the positions of the resonances as obtained by solving Eq. (3.27); from right to left n increases from 1 to 10.

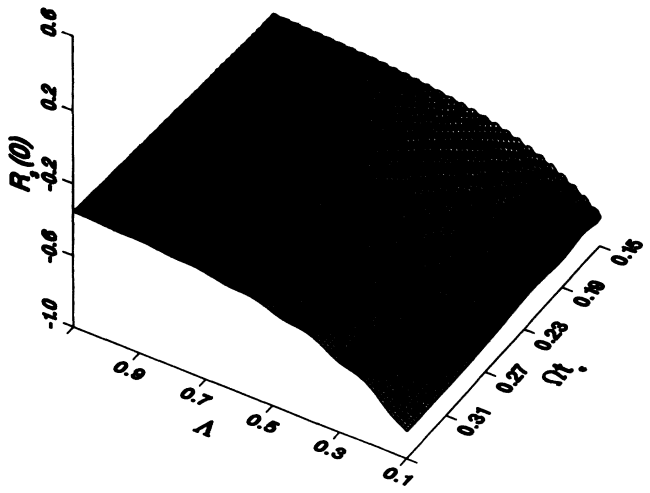

FIG. 13. This surface plots shows the average inversion $R_3(0)$ as a function of the parameters Λ and Ωt_c. The other parameters are $\gamma=\Omega$ and $\Delta\omega=0$. A low enough value of γ has been used to ensure some interference between the crossings, which is seen here as ripples in the surface. The solutions of Eq. (3.27) have been projected onto the surface; these are the lines following the valleys.

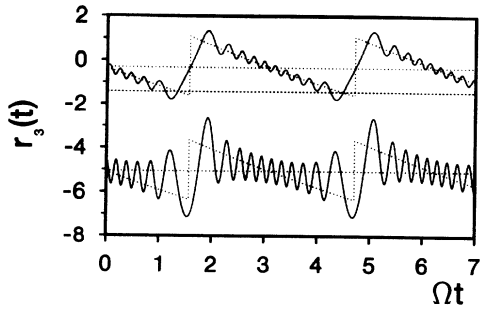

FIG. 14. We show two examples of two-dependent behavior with parameters referring to two points in Fig. 12. The solid curves give the result of numerical integration; the lower curve for $\Omega t_c=0.115\,15$ and the upper curve for $\Omega t_c=0.118\,20$. Other parameters are $\Lambda=0.22$, $\gamma=0.1\Omega$, and $\Delta\omega=0$. The two sets of parameters fall near two extrema on the $\gamma=0.1\Omega$ curve in Fig. 12. The horizontal dashed line is the estimate of the simple theory from Eq. (3.18) for the parameters of this figure (this approximation does not have any dependence on Ωt_c). The two dotted horizontal lines show the exact averages as calculated from the continued-fraction expression. The two dotted-sawtooth curves are derived from Eq. (3.13) of the simple theory by shifting the result so that their averages coincide with their exact values.

by arrows in Fig. 12. The discrepancy between the positions estimated in this way and those that are calculated can be explained by the phase shift impressed during the passing of the crossing.

The functional dependence defined by Eq. (3.24) can be simplified in various limits. If the crossing lasts only a fraction of the period $\Omega t_c \ll 1$, we have $\mathcal{E}(1)=1$ and find

$$\Lambda \simeq n\frac{\pi}{2}(\Omega t_c)^2 . \tag{3.28}$$

In the opposite limit, $\Omega t_c \gg 1$, $\mathcal{E}(\kappa)\Longrightarrow(\pi/2)$, and we find

$$\Lambda \simeq n\,\Omega t_c . \tag{3.29}$$

The results (3.28) and (3.29) determine the behavior of the lines in Fig. 13 at small and large values of Ωt_c.

Because the phase Φ describes the number of rotations of the Bloch vector, it can be used to predict the number of oscillations in the inversion over the half-cycle between the crossings; in Figs. 5 and 6 we predict about 56 oscillations. In general, if such an estimate indicates that only a few oscillations occur, the damped exponential behavior of our simple model is not expected to be seen even for small values of Ωt_c.

In Fig. 14 we show the situation where 11 cycles are expected. The lower curve is for a value of Ωt_c such that we are in a dip of the resonant transfer (cf. Fig. 12). The average inversion is depressed by the phase interference between the crossings. The upper curve is for a slightly higher value of Ωt_c, which results in a large mean value of the inversion. Now we can discern only 10 oscillations between the crossings, and their amplitudes are much smaller than those occurring near the valleys in the average transfer. This is a general feature of the interference phenomenon. Both parts of the figure show also the time dependence deriving from the simple approximation of Sec. III C as well as the averaged populations. In each case, the approximation has been shifted to make the averages agree, as was explained in connection with Fig. 5. Except for the rounding off at the level-crossing points, the approximate results represent a coarse-grained description of the time evolution.

IV. CONCLUSION

We have introduced a model two-level system with a periodically modulated energy difference on the diagonals. In particular we have looked at the situation where there are repeated level crossings with adiabatic mixing of the levels. The steady state has been investigated by exact numerical integration as well as by the use of a Fourier expansion leading to a treatment in terms of matrix-continued fractions. We have also utilized simple analytical models based on the Landau-Zener treatment of the crossings, population relaxation, and adiabatic following of the Bloch vector. The exact results have been interpreted with reference to these models, and their validity and shortcomings have been elucidated.

The problem contains several time scales of fundamental physical significance. There is the basic period imposed by the oscillational frequency Ω. This we have often represented by the equivalent parameter $T_{1/2}=\pi/\Omega$, which gives the time between consecutive level crossings. Its relation to the decay rate γ_0 tells us whether the evolution retains any memory from one crossing to the next. In the Landau-Zener treatment, the mixing of the levels can be considered to occur mainly within a time t_c defined in (3.6). From these three time scales we can form three-dimensionless parameters

characterizing the physics, but they are naturally not independent. Only two are actually needed in addition to the adiabaticity parameter Λ, which enters independently.

The intuitive understanding of the physical situation is simplified in the following limits. (a) The crossing time is short compared with the period

$$\Omega t_c = \pi t_c / T_{1/2} < 1 \ .$$

(b) The decay has little effect during the crossing time

$$\gamma_0 t_c < 1 \ .$$

(c) The decay nearly has time to run its full course during one period

$$\gamma_0 T_{1/2} = \gamma_0 \pi / \Omega > 1 \ .$$

These conditions are compatible, and we thus find the simplest behavior when

$$\Omega t_c < \gamma_0 t_c < 1 < \gamma_0 / \Omega < 1 / \Omega t_c \ . \tag{4.1}$$

A physically interesting case is obtained when we reverse condition (c) in order to introduce interference between the crossings, such as we considered in Sec. III C. Conditions (a) and (b) still hold. We then have

$$\gamma_0 / \Omega < 1 < 1 / \Omega t_c, \quad \gamma_0 t_c < \Omega t_c < 1 \ . \tag{4.2}$$

The principal phenomenon under investigation thus occurs when both conditions (a) and (b) are satisfied. The violation of (b) only obscures the population transfer at the crossings. The violation of condition (a) is more serious; then each crossing region with its strong mixing of the levels extends to the next crossing, and no simple interpretation of the behavior can be expected to hold. The need to impose condition (c) depends on whether or not we wish to avoid interference between consecutive level crossings. The conditions above have been defined in terms of the population decay rate γ_0. In the calculations we have assumed only one relaxation rate $\gamma_0 = \gamma$. In most cases of interest the coherence decay rate γ will differ from the population decay rate γ_0 by at most a factor of 2. Our physical conclusions are not affected by this.

In conclusion, we find that our model system displays several interesting physical phenomena that can be computed exactly from the Hamiltonian and interpreted in terms of simple intuitively transparent physical concepts. It is also possible that some of these effects could be investigated in real physical systems.

APPENDIX

Using the vector notation (2.9) we can write the equations (2.6)–(2.8) in the form

$$\underline{Q}_n \mathbf{R}_n = A(\mathbf{R}_{n+1} + \mathbf{R}_{n-1}) + \frac{2V\lambda_p}{in\Omega + \gamma_0} \begin{bmatrix} 1 \\ 0 \end{bmatrix} \delta_{n0} \ , \tag{A1}$$

where the matrix $\underline{Q}_n$ is given by

$$\underline{Q}_n = \begin{bmatrix} -2\Delta\omega & in\Omega + \gamma + \dfrac{4V^2}{in\Omega + \gamma_0} \\ -(in\Omega + \gamma) & -2\Delta\omega \end{bmatrix} . \tag{A2}$$

Multiplying (A1) from the left with $\underline{Q}_n^{-1}$ we obtain Eq. (2.10) with

$$\begin{aligned} \mathbf{B} &= \frac{2V\lambda_p}{\gamma_0} \underline{Q}_0^{-1} \begin{bmatrix} 1 \\ 0 \end{bmatrix} \\ &= \frac{2V\lambda_p}{\gamma_0} \frac{1}{4\Delta\omega^2 + \gamma^2 + 4V^2\gamma/\gamma_0} \begin{bmatrix} -2\Delta\omega \\ \gamma \end{bmatrix} \end{aligned} \tag{A3}$$

and

$$\underline{C}_n = A \underline{Q}_n^{-1} \ . \tag{A4}$$

With the transfer matrices $\underline{T}_n$ defined in Eq. (2.11) we find the recurrence relations

$$\delta_{n0} \underline{T}_0^{-1} + \underline{C}_n (\underline{T}_{n+1} + \underline{T}_{n-1}) \underline{T}_n^{-1} = \underline{1} \ . \tag{A5}$$

We can solve these equations in terms of continued fractions by introducing

$$\underline{F}_k^{\pm} = \underline{T}_{k\pm1} \underline{T}_k^{-1} \ . \tag{A6}$$

Solving (A5) for $n \geq 0$ we write

$$\underline{F}_{n-1}^{+} = (\underline{1} - \underline{C}_n \underline{F}_n^{+})^{-1} \underline{C}_n \tag{A7}$$

and for $n \leq 0$

$$\underline{F}_{n+1}^{-} = (\underline{1} - \underline{C}_n \underline{F}_n^{-})^{-1} \underline{C}_n \ . \tag{A8}$$

These relations can be iterated to produced continued fractions; thus for $n = 1$ we find from (A7)

$$\underline{F}_0^{+} = \cfrac{1}{\underline{1} - \underline{C}_1 \cfrac{1}{\underline{1} - \underline{C}_2 \cfrac{1}{\underline{1} - \underline{C}_3 \cfrac{1}{\underline{1} - \underline{C}_4 \cfrac{1}{\underline{1} - \cdots}\underline{C}_4}\underline{C}_3}\underline{C}_2}\underline{C}_1} \tag{A9}$$

All factors here are matrices and hence their order must be retained. The matrix $\underline{F}_0^{-}$ can be obtained from (A8) in a similar form; the matrices $\underline{C}_n$ have only to be replaced by $\underline{C}_{-n}$. Introducing these expressions into (A5) with $n = 0$, we obtain the solution

$$\underline{T}_0 = [\underline{1} - \underline{C}_0 (\underline{F}_0^{+} + \underline{F}_0^{-})]^{-1} \ . \tag{A10}$$

Knowing $\underline{T}_0$ we can obtain $\underline{T}_{\pm1}$ from $\underline{F}_0^{\pm}$, and then the

matrices $\underline{T}_n$ for larger values of n can, in principle, be obtained from the recurrence relation (A5). This procedure is, however, numerically unstable, because the desired convergent solution for the Fourier coefficients is drowned by the admixture of a divergent solution. (See the discussion in Ref. [13].) Thus we have evaluated the transfer matrices from the expressions

$$\underline{T}_n=\underline{F}^{+}_{n-1}\underline{F}^{+}_{n-2}\underline{F}^{+}_{n-3}\cdots\underline{F}^{+}_{2}\underline{F}^{+}_{1}\underline{T}_0 \tag{A11}$$

for $n>0$; for $n<0$, we use the matrices $\underline{F}^{-}_{n}$ in a similar fashion. The matrices $\underline{F}^{\pm}_{n}$ are obtained by evaluating continued fractions of the type (A9). This approach to evaluate the matrices has been found to be stable in all cases treated. Knowing the matrices $\underline{T}_n$ we can obtain the Fourier components $\mathbf{R}_n$ from Eq. (2.11).

The continued fraction (A9) can be evaluated by truncation and multiplication up. However, this method is inefficient and time consuming because many operations are needed to ensure convergence, and previous results are not used in later computations. Adopting the algorithm by Abramowitz and Stegun [13] for scalar fractions to our matrix case, we find that the matrix (A9) can be obtained in the form

$$\underline{F}^{+}_{n}=\underline{A}_n\underline{B}^{-1}_{n}, \tag{A12}$$

where $\{\underline{A}_n\}$ and $\{\underline{B}_n\}$ are two independent solutions of the matrix equations

$$\underline{X}_n=(\underline{X}_{n-1}+\underline{X}_{n-2}\underline{C}_{n-1})\underline{C}^{-1}_{n+1}. \tag{A13}$$

The two solutions are determined by the initial conditions

$$\underline{A}_{-1}=\underline{1},\quad \underline{A}_0=\underline{0}, \tag{A14}$$

$$\underline{B}_{-1}=\underline{0},\quad \underline{B}_0=\underline{C}^{-1}_{1}. \tag{A15}$$

With these, the consecutive approximations to (A12) can be obtained in succession until desired accuracy is reached. To calculate $\underline{F}^{-1}_{n}$ we use a similar scheme but replace $\underline{C}_n$ by $\underline{C}_{-n}$ throughout the calculation.

[1] L. D. Landau, Phys. Z. Sowjetunion **2**, 46 (1932).

[2] C. Zener, Proc. R. Soc. London, Ser. A **137**, 696 (1932).

[3] S. Stenholm, *Applications of Lasers in Atomic, Molecular and Nuclear Physics,* Proceedings of the Second School on Laser Applications in Atomic, Molecular and Nuclear Physics, Vilnius, 1981 (Nauka, Moscow, 1983), p. 60.

[4] S. Stenholm, in *Quantum Optics, Experimental Gravitation, and Measurement Theory,* edited by P. Meystre and M. O. Scully (Plenum, New York, 1983), p. 117.

[5] R. J. C. Spreeuw, J. P. Woerdman, and D. Lenstra, Phys. Rev. Lett. **61**, 318 (1988).

[6] R. J. C. Spreeuw, E. R. Eliel, and J. P. Woerdman, Opt. Commun. **75**, 141 (1990).

[7] A. P. Kazantsev, V. S. Smirnov, G. I. Surdutovich, D. O. Chudesnikov, and V. P. Yakovlev, J. Opt. Soc. Am. B **2**, 1731 (1985).

[8] J. Dalibard and C. Cohen-Tannoudji, J. Opt. Soc. Am. B **6**, 2023 (1989).

[9] D. J. Fernandez and B. Mielnik, Phys. Rev. **41**, 5788 (1990).

[10] R. C. Stoneman, D. S. Thomson, and T. F. Gallagher, Phys. Rev. A **37**, 1527 (1988).

[11] W. H. Press, B. P. Flannery, S. A. Teukolsky, and W. T. Vetterling, *Numerical Recipes* (Cambridge University, Cambridge, 1986).

[12] H. Risken, *The Fokker-Planck Equation* (Springer-Verlag, Heidelberg, 1984).

[13] *Handbook of Mathematical Functions with Formulas, Graphs and Mathematical Tables,* Natl. Bur. Stand. Appl. Math. Ser. No. 55, edited by M. Abramowitz and I. A. Stegun (U.S. GPO, Washington, DC, 1965), pp. XIII and 19.

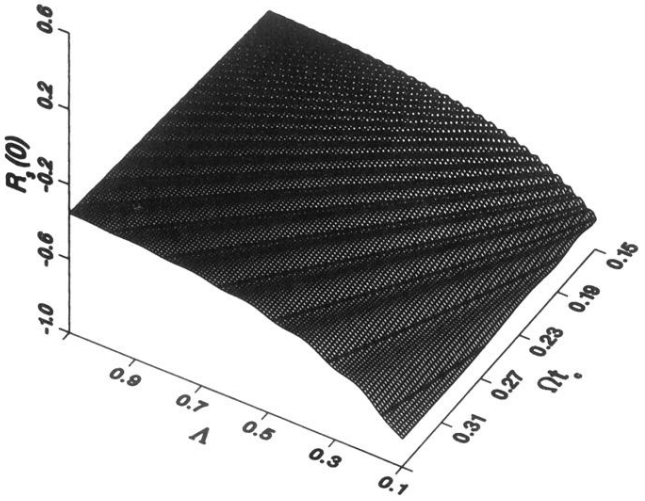

FIG. 13. This surface plots shows the average inversion $R_3(0)$ as a function of the parameters Λ and Ωt_c. The other parameters are $\gamma=\Omega$ and $\Delta\omega=0$. A low enough value of γ has been used to ensure some interference between the crossings, which is seen here as ripples in the surface. The solutions of Eq. (3.27) have been projected onto the surface; these are the lines following the valleys.